NANO LETTERS
Letter
Cite This: Nano Lett. 2019, 19, 1124−1130
pubs.acs.org/NanoLett

Bifacial Raman Enhancement on Monolayer Two-Dimensional Materials

Na Zhang,[†] Jingjing Lin,[†] Wei Hu,[‡,⊥] Shuqing Zhang,[†] Liangbo Liang,[§] Rui Wang,[∥] Xue Luo,[†] Yi Luo,[‡] Xiaohui Qiu,[∥] Jin Zhang,[†] and Lianming Tong*[,†]

[†]Center for Nanochemistry, Beijing Science and Engineering Center for Nanocarbons, Beijing National Laboratory for Molecular Sciences, College of Chemistry and Molecular Engineering, Peking University, Beijing 100871, People's Republic of China

[‡]Hefei National Laboratory for Physical Science at the Microscale and Synergetic Innovation Center of Quantum Information & Quantum Physics, University of Science and Technology of China, Hefei, Anhui 230026, People's Republic of China

[§]Center for Nanophase Materials Sciences, Oak Ridge National Laboratory, Oak Ridge, Tennessee 37831, United States

[∥]National Center for Nanoscience and Technology, Chinese Academy of Sciences, Beijing 100190, People's Republic of China

Supporting Information

ABSTRACT: Understanding the charge interaction between molecules and two-dimensional (2D) materials is essential for the design of functional devices. Here, we report the bifacial Raman enhancement of molecules on monolayer graphene and hexagonal boron nitride (*h*-BN). Taking advantage of the atomically thick layered structure, we show that both surfaces of 2D materials can interact with molecules and simultaneously enhance their Raman scattering. Different enhancement features were observed for monolayer graphene and *h*-BN. The intensity decrease of particular Raman modes of copper phthalocyanine (CuPc) on both surfaces of *h*-BN suggests that *z*-dipoles exist and are partially canceled out between the two interfaces, while the twice Raman intensities of the characteristic Raman modes of CuPc on both surfaces of graphene compared to that on one surface evidenced the charge transfer process. These results provide an approach to modify 2D materials by bifacial adsorption of molecules, and the findings can inspire the design of functional 2D material-based devices.

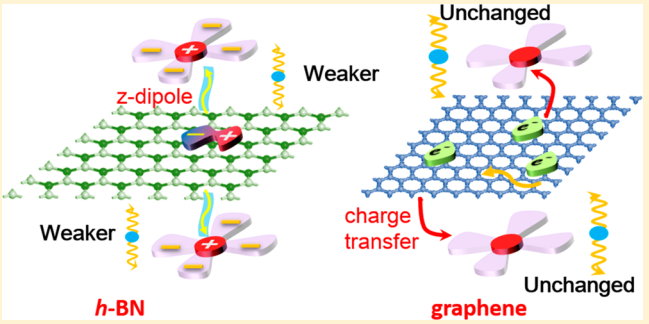

KEYWORDS: *Bifacial Raman enhancement, charge interactions, Raman scattering, two-dimensional materials*

Raman enhancement effect on two-dimensional (2D) layered materials has been extensively investigated.[1] The mechanism of enhancement is attributed to a pure chemical effect due to the lack of surface plasmons in the visible light region, and the Raman enhancement effect has been observed on a number of 2D layered materials, including graphene,[2] hexagonal boron nitride (*h*-BN), molybdenum disulfide (MoS_2),[3] gallium selenide (GaSe),[4] heterostructure of tungsten disulfide (WS_2) and graphene,[5] and anisotropic black phosphorus (BP) and rhenium disulfide (ReS_2).[6] The chemical enhancement requires the physical contact between molecules and material, so that charge interactions can occur at the interface that modulates the effective polarizability of the molecules and leads to the amplification of the Raman signals.[7,8] Interestingly, monolayer 2D materials have two surfaces that can both provide channels for effective charge interactions with molecules. The two-faced layered feature has been used for asymmetric functionalization and synthetic of Janus monolayers of graphene and transition metal dichalcogenides (TMDs), which are of great potential for diverse optoelectronic and sensing applications.[9−14] For molecules adsorbed on the two surfaces of a monolayer 2D material, the charge interactions occur between molecules and the material at the two interfaces, which may interfere with each other depending on the property of the material and the form of charge interactions. The understanding of such interactions would also be helpful for the design and optimization of molecules/2D materials heterostructures.

In this regard, we show the bifacial Raman enhancement of molecules by monolayer graphene and *h*-BN. Copper phthalocyanine (CuPc) was used as probe molecules. Utilizing the molecular fingerprint recognition and the enhanced Raman scattering intensities, different roles of dielectric *h*-BN and semimetallic graphene were clearly observed. It was found that for *h*-BN, adding a second monolayer of molecules on the other side results in an increase of Raman intensity that is less than that of the single-layer molecules, and certain Raman modes are preferentially suppressed. This was attributed to the formation of *z*-dipoles between *h*-BN and CuPc, which interfere each other at both interfaces. However, for graphene,

Received: November 3, 2018
Revised: January 8, 2019
Published: January 24, 2019

DOI: 10.1021/acs.nanolett.8b04433
Nano Lett. 2019, 19, 1124−1130

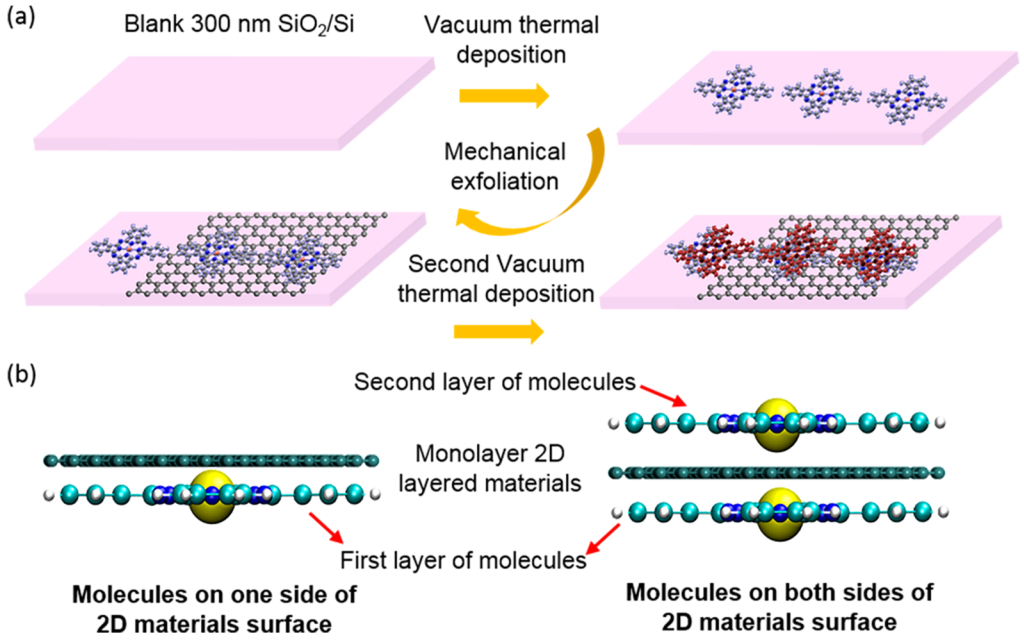

Figure 1. (a) Schematic procedure of sample preparation. (b) Schematics of molecules on one surface and both surfaces of a monolayer 2D material.

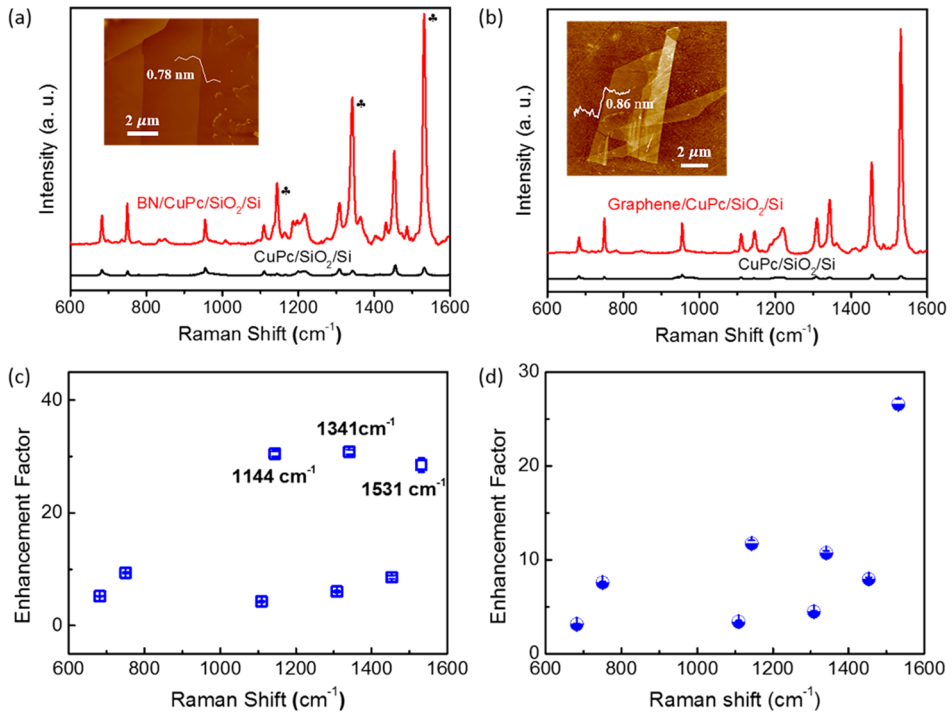

Figure 2. Raman spectra of CuPc molecules under monolayer *h*-BN (a) and graphene (b). The insets are the corresponding AFM images. The enhancement factors for different vibrational modes in monolayer *h*-BN/CuPc/SiO_2/Si (c) and monolayer graphene/CuPc/SiO_2/Si (d).

the increase of Raman intensity was almost equal to that of molecules on one surface owing to the charge transfer between CuPc and graphene. These results were further confirmed by optical absorption measurements and theoretical calculations. The layer number dependence of the Raman enhancement was also studied, and the different thickness dependence of Raman intensities agreed well with the proposed model.

Results and Discussion. The preparation of samples was schematically shown in Figure 1. CuPc molecules were first deposited on a 300 nm SiO_2/Si substrate through vacuum thermal evaporation, and the thickness of the deposited molecules was around 3 Å, corresponding to no more than monolayer coverage.[3] Monolayer graphene or *h*-BN was then transferred on the top of molecules by mechanical exfoliation. Raman scattering measurements of the single-layer CuPc molecules were performed, and the Raman enhancement of molecules by graphene and *h*-BN was clearly seen in Figure 2. Next, the same amount of CuPc molecules was deposited on the top of monolayer graphene or *h*-BN for further measurements of bifacial Raman enhancement.

DOI: 10.1021/acs.nanolett.8b04433
Nano Lett. 2019, 19, 1124−1130

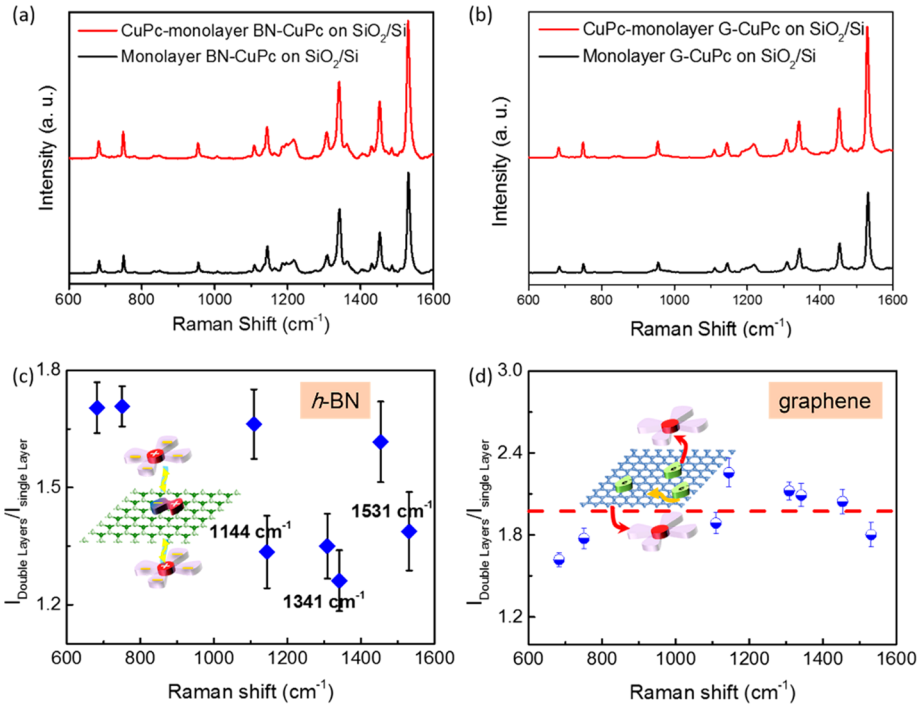

Figure 3. Raman spectra of double-layer CuPc molecules and single-layer CuPc molecules contacted with monolayer *h*-BN (a) and graphene (b). The extracted Raman intensity ratios of double-layer versus single-layer CuPc molecules on monolayer *h*-BN (c) and graphene (d).

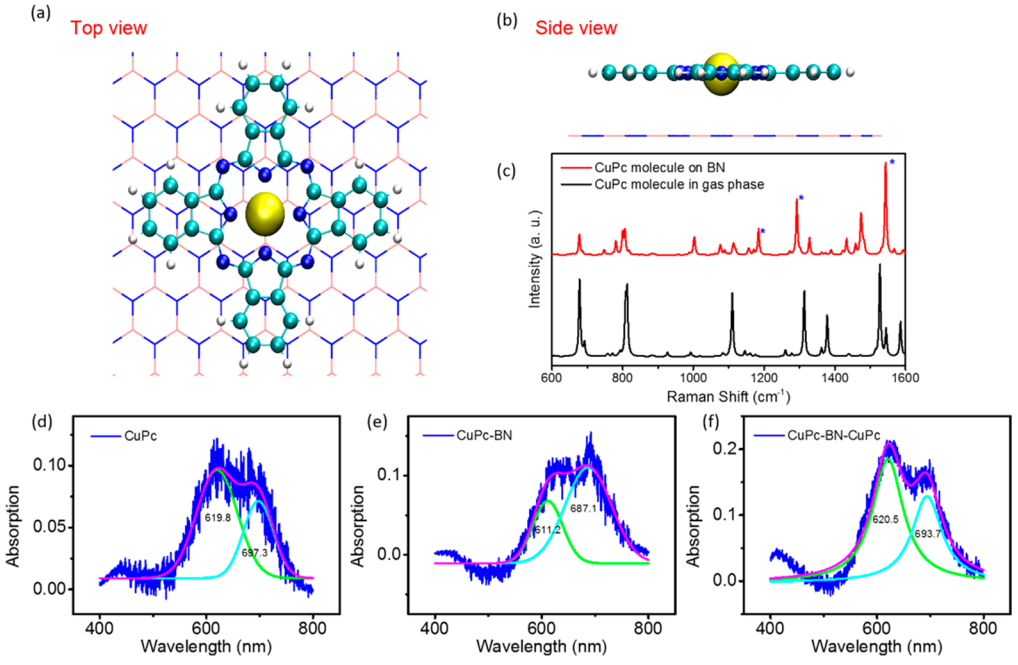

Figure 4. Top view (a) and side view (b) of CuPc molecule adsorbed on *h*-BN. (c) Calculated Raman spectra of CuPc molecules in the gas phase (black line) and on BN (red line) with normalized intensities. Comparison of the absorption spectra of CuPc molecules on a blank quartz substrate (d), CuPc molecules on one side of the monolayer BN flake (e), and CuPc molecules on both sides of the monolayer BN flake (f).

All of the Raman spectra were collected using a 632.8 nm excitation laser, which is in resonance with CuPc molecules. As shown in Figure 2a,b, the Raman intensities of CuPc underneath monolayer *h*-BN and graphene were both enhanced compared with those on the blank SiO_2/Si substrate. The enhancement factors (EFs) could reach 31 and 27, respectively. It can be seen that the Raman enhancement characteristics of CuPc molecules are different on *h*-BN and graphene. For *h*-BN, the Raman modes at 1144, 1341, and 1531 cm^{-1} were preferentially enhanced compared to other modes, such as the peaks at 682, 749, 1109, 1306, and 1452 cm^{-1} (Figure 2c). As shown in Table S1 (see Supporting Information), the modes at 1144, 1341, and 1531 cm^{-1} were related to the displacement of N atoms, particularly the N atoms bonding to the Cu atom at the center, consistent with references.[15,16] Although the Raman mode at 1306 cm^{-1} is also

DOI: 10.1021/acs.nanolett.8b04433
Nano Lett. 2019, 19, 1124−1130

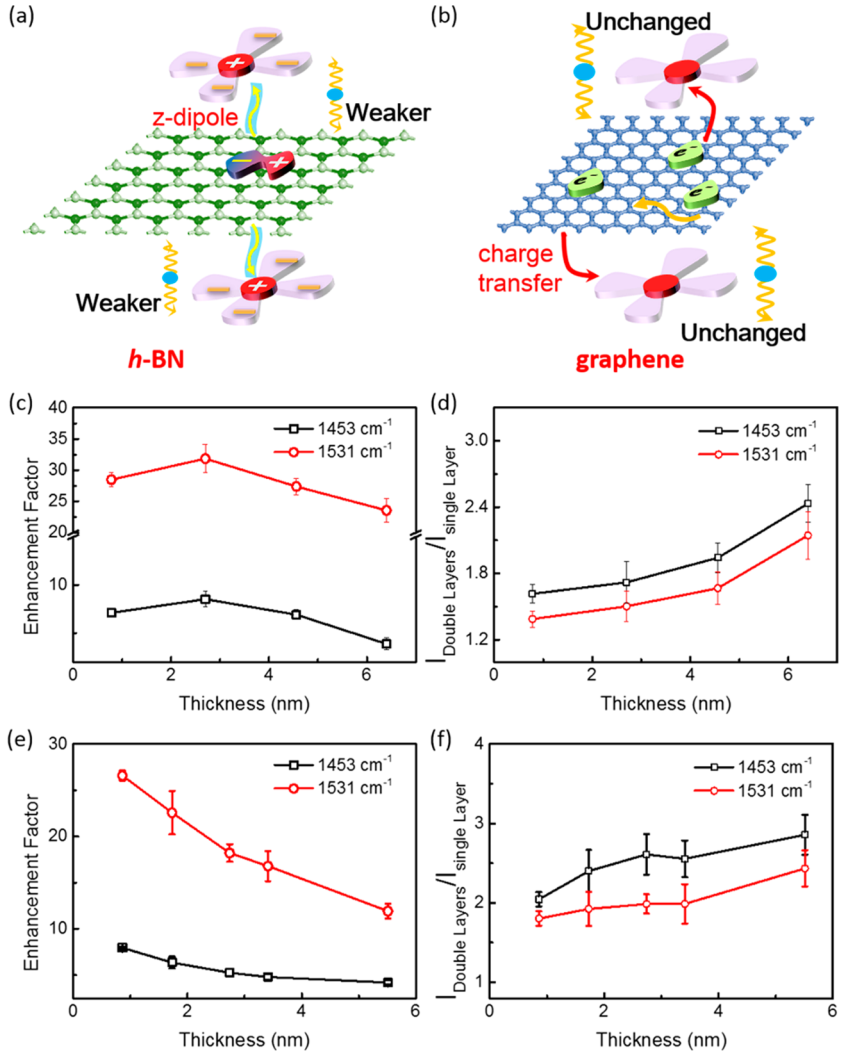

Figure 5. Schematic picture of the bifacial Raman enhancement on monolayer *h*-BN (a) and graphene (b). The enhancement factors for Raman modes at 1453 and 1530 cm^{-1} with the increase of thickness of *h*-BN (c) and graphene (e). The Raman intensity ratios of a double layer versus single layer for vibration modes of 1453 and 1530 cm^{-1} of CuPc molecules with the increase of thickness of *h*-BN (d) and graphene (f).

related to the displacement of N atoms, it belongs to the asymmetric stretching and does not lead to significant change of the total polarization of CuPc as well as the interaction between CuPc and *h*-BN, and thus the peak does not show remarkable enhancement. Hence, it can be concluded that the vibrational modes with a large polarization change exhibit a more effective Raman enhancement. While for that on graphene, the enhancement factors of different Raman modes of CuPc increased pseudo linearly with Raman frequency (Figure 2d), owing to the better alignment of energy band for the modes with higher frequencies.[17,18] The pump−probe measurements also suggested that the charge transfer occurs in the interface of CuPc/graphene (Figure S1).

CuPc molecules can interact with *h*-BN via a dipole−dipole interaction.[3] The charge transfer between molecules and *h*-BN is unlikely because *h*-BN is an insulator with a large band gap of ∼5.9 eV, and the energy band structure does not match that of molecules. If there are molecules on both surfaces of *h*-BN, the dipoles will be enhanced or canceled out. The amount of molecules was confirmed to be the same on both surfaces by Raman scattering intensities and XPS measurements (Figures S2 and S3), thus the bifacial Raman enhancement (double-layer, DL) of CuPc molecules was normalized by the enhancement of single-layer (SL) molecules for a better comparison. As shown in Figure 3a,c, the enhancement averaged by all of the Raman modes of DL CuPc molecules was estimated to be ∼1.5 compared to that of SL ones on *h*-BN. More interestingly, the Raman modes that were preferentially enhanced for SL CuPc molecules (Figure 2c) showed a significantly lower enhancement for DL molecules (reduced by ∼35%, see Figure 3c). While for graphene, the intensity ratios of DL/SL CuPc molecules were ∼2.0 for all of the Raman modes (Figure 3b,d). For monolayer graphene, due to the high conductivity and free carrier density, the charge transfer between molecules and graphene is expected to be the same at both interfaces. These results suggest that *h*-BN and graphene play different roles in the bifacial Raman enhancement.

DFT calculations showed that the total energy for CuPc/*h*-BN was the lowest when the Cu atom in CuPc was placed on the top of an N atom, and the major axis of CuPc was along the zigzag and armchair directions (rotation angle 30°, Figure 4a,b and Table S2). As N atoms in *h*-BN have lone pair electrons, dipoles are formed along the *z*-direction between N atoms and Cu atoms, and the dipole moment was calculated to be 1.2×10^{-2} Debye. Under this adsorption configuration, the

DOI: 10.1021/acs.nanolett.8b04433
Nano Lett. 2019, 19, 1124−1130

calculated enhanced Raman spectrum of CuPc exhibits a good agreement with experimental results, where preferentially enhanced Raman modes that are relevant to the N atoms bonding to Cu in CuPc molecules have a larger polarizability change,[19,20] as indicated in Figure 4c. However, with a second monolayer molecules adsorbed with the same configuration on the other side of *h*-BN, the *z*-dipole was reduced and the dipole moment was weakened to be 2.1×10^{-3} Debye. This can be attributed to the competitive formation of N → Cu dipole on the top of *h*-BN and Cu ← N dipoles on the other side. The detailed estimation of surface coverage of CuPc molecules is given in the Supporting Information.

Optical absorption of CuPc molecules on a fused quartz substrate, CuPc/*h*-BN/quartz and CuPc/*h*-BN/CuPc/quartz samples was also measured and shown in Figure 4d–f. For phthalocyanine derivatives, the Q-band is ascribed to $\pi \rightarrow \pi^*$ excitation between bonding and antibonding molecular orbitals and can be well distinguished in the visible region.[21,22] The two peaks observed in Figure 4d–f were attributed to the aggregated states (at about 620 nm, named Q1) and monometric states (at about 697 nm, named Q2), respectively.[23] CuPc molecules on a fused silica substrate showed characteristic Q1 and Q2 bands at about 619.8 and 697.8 nm, while the bands blue shifted to 611.2 and 687.1 nm if the molecules are on *h*-BN, which is due to the dipole formation between Cu and N in *h*-BN.[23,24] The change of relative intensities probably originated from the better coupling of the molecules in monometric states to *h*-BN than those in aggregated states. After the second deposition of CuPc molecules on the top surface of *h*-BN, the Q1 and Q2 bands shifted to 620.5 and 693.7 nm (Figure 4f), which were close to that on a quartz substrate, indicating the much weakened dipolar interactions between CuPc and *h*-BN, in consistence with the competitive formation of N → Cu dipole on the top of *h*-BN and Cu ← N dipoles on the other surface. An N atom in *h*-BN shares its lone pair electrons to form two dipoles. Thus, the effective charges are reduced and the dipoles are weakened (Figure 5a), leading to less than twice of the overall enhancement ($I_{DL}/I_{SL} \sim 1.5$, see Figure 3c), and the Raman modes related to the displacement of N atoms bonding to Cu in CuPc (1140, 1340, 1530 cm^{-1}) are further weakened. On the contrary, the optical absorption of the CuPc molecule on both surfaces of graphene showed only a slight change compared to that of molecules on one surface, as shown in Figure S4, which evidenced that the charge transfer between molecules and graphene was not affected by the deposition of CuPc on the other surface (Figure 5b), leading to twice the overall enhancement of 2L CuPc molecules.

The thickness-dependent enhancement factors (EFs) of CuPc molecules underneath *h*-BN and graphene were shown in Figure 5c,e. As the thickness of the materials increased, the EF of molecules underneath graphene decreased monotonically because of the increased absorption of the incident photons and scattering photons by graphene (Figure 5e), while the EF in the *h*-BN system had a maximum at around 4 layers and then fell off slowly (Figure 5c). This can be ascribed to the competition between optical effect of the increased thickness of *h*-BN and the additional Raman enhancement from the accessional *h*-BN layers. For molecules on both surfaces of *h*-BN, the relative enhancement (I_{DL}/I_{SL}) increased with the thickness of *h*-BN (Figure 5d), confirming that, by increasing the number of layers of *h*-BN, the *z*-dipoles are less affected by the molecules on the other side. However, the screening effect of graphene still holds for increased layer numbers, so the relative enhancement (I_{DL}/I_{SL}) only increased slightly (Figure 5f), probably owing to the loss of incident and scattered photons of the molecules underneath graphene.

Conclusions. In summary, a bifacial Raman enhancement on monolayer graphene and *h*-BN was studied. For copper phthalocyanine (CuPc) molecules on monolayer *h*-BN, *z*-dipoles formed between Cu and N in *h*-BN are responsible for the preferential enhancement of the Raman modes with a larger polarization, and the intensity reduction of these Raman modes for CuPc on both sides is ascribed to the partial cancellation of *z*-dipoles at the two surfaces of *h*-BN. The Raman intensities of molecules on both surfaces of graphene are twice that of molecules on one side due to the charge transfer and adequate free electrons in graphene. This model was further confirmed by optical absorption spectroscopy and DFT calculations. The layer number dependence of Raman intensities on graphene and *h*-BN agreed well with the proposed model. This work provides the avenue to further study the charge interaction between molecules and 2D layered materials through enhanced Raman scattering spectroscopy and may inspire a rational design of potential 2D material-based functional molecular devices.

Experimental Section. *Preparation of the Samples.* Graphene and *h*-BN were prepared by mechanical exfoliation onto a clean 300 nm SiO_2/Si substrate. The sample was characterized by optical microscopy (OM), atom force microscopy (AFM), and Raman spectroscopy. CuPc molecules were deposited on the substrate by a standard thermal evaporator. The base pressure for deposition was about 1×10^{-6} Torr. The evaporation current was about 66 A. The thickness of the CuPc molecules was monitored using a fused silica crystal monitor, and the typical thickness was around 3 Å.

Raman Measurements. Raman measurements were carried out using a Horiba–Jobin Yvon system with a 632.8 nm He–Ne laser line. The laser power was around 1 mW on the sample, and the size of the laser beam on the sample was around 1 μm^2 focused by a 100× objective. The typical exposure time was 5 s. All spectra were averaged with three measurements on different spots of the samples. The Raman peaks were fitted by a Lorenzian–Gaussian function using the LabSpec software to obtain the Raman shifts, intensity, and full width at the half-maximum intensity.

Optical Absorption Measurements. The optical absorption of the CuPc molecules on fused silica was measured on a Witec RSA300+ optical microscope. The substrate was illuminated by a KL 1500 halogen lamp (Zeiss) in transmission mode, with a 100× objective lens to focus the incident light and 60× objective lens to collect the signal. The absorbance (A) was calculated as $A = \ln(I_0/I)$, where I is the light intensity transmitted through the detection spot, and I_0 is the light intensity transmitted through the blank fused silica substrate.

XPS Characterization. The XPS measurement was carried out using Axis Supra/Ultra with an Al Kα X-ray source ($\hbar\nu$ = 1486.7 eV). The energy calibrations were made against the C 1s peak to eliminate the charging of the sample during analysis.

Temporally Resolved Pump–Probe Measurements. A pump pulse with a 390 nm wavelength and 200 fs temporal width was focused on the sample to a spot size of about 2 μm. The probe pulse with 650 nm and 200 fs pulse duration was focused by the same lens, and its reflection was collected and detected by a photodetector, the output of which was amplified by a lock-in amplifier. The pump and probe pulses were both

DOI: 10.1021/acs.nanolett.8b04433
Nano Lett. 2019, 19, 1124–1130

linearly polarized along perpendicular directions. A mechanical chopper modulates the pump beam at ~1.3 kHz for lock-in detection. Reflection and scattering of the pump beam were prevented from reaching the photodetector by using long pass filters. In this configuration, the lock-in amplifier measures the change in the reflection of the probe pulse from the sample induced by the pump (i.e., ΔR). Such a quantity was then normalized to provide a differential reflection, i.e., $\Delta R/R_0 = (R - R_0)/R_0$, where R and R_0 are the reflection of the probe pulse from the sample with and without the presence of the pump pulse, respectively. All measurements were carried out under ambient conditions and at room temperature.

Calculation Methods. The geometries of the CuPc molecules on *h*-BN systems are optimized using the periodic boundary condition (PBC) model implemented in the Vienna ab initio simulation package (VASP).[25] The 30 Å × 30 Å *h*-BN slab layers are constructed to represent the substrate. Basically, the designed supercell has enough surface area to accommodate the CuPc molecules. For the k-point sampling, only the Γ point is adopted. The final forces on CuPc atoms are less than 0.02 eV Å^{-1}. Projector augmented wave pseudopotentials are employed to represent the interaction between the core ions and the valence electrons. On the other hand, the vdW correction is evaluated using vdW-D3 method.[26] Based on the optimized geometries, the Raman spectrum is simulated using our previously developed quasi-analytical method with dispersion correction (QAD).[27,28] To be specific, a dynamical matrix of the system is generated by displacing each atom of CuPc along each Cartesian direction by 0.01 Å. Further diagonalization of the truncated dynamical matrix produces vibrational frequencies and corresponding phonon eigenvectors *lik*. Then according to the chain rule, the Raman tensor can be written as

$$R^k_{\alpha\beta} = \sum_i \frac{l_{ik}}{\sqrt{m_i}} \frac{\partial F_i}{\partial \varepsilon_\alpha \partial \varepsilon_\beta}$$

where m is the mass of the atom, ε is the external electric field, α and β represent Cartesian directions, and F is the force vector and can be calculated analytically. The second derivative of F can be effectively computed using the second-order finite-difference method (the central-difference formula). With the calculated Raman tensors, differential Raman cross sections can be calculated using the standard expression[29]

$$\left(\frac{d\sigma}{d\Omega}\right)_k = \frac{\pi^2}{\varepsilon_0^2}(\tilde{\nu}_{in} - \tilde{\nu}_k)^4 \frac{h}{8\pi^2 c\tilde{\nu}_k} \times |\vec{e}_i \cdot \hat{R} \cdot \vec{e}_s|^2 \frac{1}{1 - \exp(-hc\tilde{\nu}_k/k_B T)}$$

where the wavelength of the incident light and the temperature are set to be 632.8 nm and 300 K, respectively. All calculated Raman cross sections are convoluted with a Lorentzian function with a full width at half-maximum of 5 cm^{-1} for comparison with experimental spectra. For assigning the vibrational modes of Raman peaks in the CuPc molecule, Gaussian 03 package[30] based on the PBE functional and 6-31G basis sets are also used in the Raman calculation.

■ ASSOCIATED CONTENT

Supporting Information

The Supporting Information is available free of charge on the ACS Publications website at DOI: 10.1021/acs.nanolett.8b04433.

Enhancement factors of different Raman modes of CuPc on different substrates, temporally resolved pump–probe measurements, Raman spectra, XPS spectra, absorption spectra, and calculated total energies of CuPc/BN under different adsorption configurations (PDF)

■ AUTHOR INFORMATION

Corresponding Author

*E-mail: tonglm@pku.edu.cn.

ORCID

Wei Hu: 0000-0002-7467-4783
Liangbo Liang: 0000-0003-1199-0049
Jin Zhang: 0000-0003-3731-8859
Lianming Tong: 0000-0001-7771-4077

Present Address

⊥School of Chemistry and Pharmaceutical Engineering, Qilu University of Technology (Shandong Academy of Sciences), Jinan 250353, People's Republic of China

Author Contributions

All authors have given approval to the final version of the manuscript.

Notes

The authors declare no competing financial interest.

■ ACKNOWLEDGMENTS

The authors thank J. Guan and X. Li for the vacuum thermal deposition. This work was supported by the National Natural Science Foundation of China (51432002, 51720105003, 21790052, 11374355, 21573004, and 11504064), the Ministry of Science and Technology of China (2016YFA0200100 and 2015CB932403), and the Beijing Municipal Science and Technology Project (Z161100002116026).

■ REFERENCES

(1) Zhang, N.; Tong, L.; Zhang, J. Graphene-based Enhanced Raman Scattering towards Analytical Applications. *Chem. Mater.* **2016**, *5* (29), 15273−15286.

(2) Ling, X.; Xie, L.; Fang, Y.; Xu, H.; Zhang, H.; Kong, J.; Dresselhaus, M. S.; Zhang, J.; Liu, Z. Can graphene be used as a substrate for Raman enhancement? *Nano Lett.* **2010**, *10* (2), 553−561.

(3) Ling, X.; Fang, W.; Lee, Y.-H.; Araujo, P. T.; Zhang, X.; Rodriguez-Nieva, J. F.; Lin, Y.; Zhang, J.; Kong, J.; Dresselhaus, M. S. Raman Enhancement Effect on Two-Dimensional Layered Materials: Graphene, h-BN and MoS2. *Nano Lett.* **2014**, *14* (6), 3033−3040.

(4) Quan, L.; Song, Y.; Lin, Y.; Zhang, G.; Dai, Y.; Wu, Y.; Jin, K.; Ding, H.; Pan, N.; Luo, Y.; Wang, X. The Raman enhancement effect on a thin GaSe flake and its thickness dependence. *J. Mater. Chem. C* **2015**, *3* (42), 11129−11134.

(5) Tan, Y.; Ma, L.; Gao, Z.; Chen, M.; Chen, F. Two-Dimensional Heterostructure as a Platform for Surface-Enhanced Raman Scattering. *Nano Lett.* **2017**, *17* (4), 2621−2626.

(6) Lin, J.; Liang, L.; Ling, X.; Zhang, S.; Mao, N.; Zhang, N.; Sumpter, B. G.; Meunier, V.; Tong, L.; Zhang, J. Enhanced Raman Scattering on In-Plane Anisotropic Layered Materials. *J. Am. Chem. Soc.* **2015**, *137* (49), 15511−15517.

(7) Schluecker, S. Surface-Enhanced Raman Spectroscopy: Concepts and Chemical Applications. *Angew. Chem., Int. Ed.* **2014**, *53* (19), 4756−4795.

(8) Ling, X.; Zhang, J. First-Layer Effect in Graphene-Enhanced Raman Scattering. *Small* **2010**, *6* (18), 2020−2025.

(9) Zhang, L.; Yu, J.; Yang, M.; Xie, Q.; Peng, H.; Liu, Z. Janus graphene from asymmetric two-dimensional chemistry. *Nat. Commun.* **2013**, *4*, 1443.

DOI: 10.1021/acs.nanolett.8b04433
Nano Lett. 2019, 19, 1124−1130

(10) Dong, L.; Lou, J.; Shenoy, V. B. Large In-Plane and Vertical Piezoelectricity in Janus Transition Metal Dichalchogenides. *ACS Nano* **2017**, *11* (8), 8242−8248.
(11) Lu, A.-Y.; Zhu, H.; Xiao, J.; Chuu, C.-P.; Han, Y.; Chiu, M.-H.; Cheng, C.-C.; Yang, C.-W.; Wei, K.-H.; Yang, Y.; et al. Janus monolayers of transition metal dichalcogenides. *Nat. Nanotechnol.* **2017**, *12* (8), 744−749.
(12) Ajayan, P.; Kim, P.; Banerjee, K. Two-dimensional van der Waals materials. *Phys. Today* **2016**, *69* (9), 38−44.
(13) Novoselov, K. S.; Mishchenko, A.; Carvalho, A.; Castro Neto, A. H. 2D materials and van der Waals heterostructures. *Science* **2016**, *353* (6298), 9439.
(14) Jariwala, D.; Marks, T. J.; Hersam, M. C. Mixed-dimensional van der Waals heterostructures. *Nat. Mater.* **2017**, *16* (2), 170−181.
(15) Liu, Z.; Zhang, X.; Zhang, Y.; Jiang, J. Theoretical investigation of the molecular, electronic structures and vibrational spectra of a series of first transition metal phthalocyanines. *Spectrochim. Acta, Part A* **2007**, *67* (5), 1232−1246.
(16) Basova, T. V.; Kiselev, V. G.; Schuster, B. E.; Peisert, H.; Chassé, T. Experimental and theoretical investigation of vibrational spectra of copper phthalocyanine: polarized single-crystal Raman spectra, isotope effect and DFT calculations. *J. Raman Spectrosc.* **2009**, *40* (12), 2080−2087.
(17) Deng, S.; Xu, W.; Wang, J.; Ling, X.; Wu, J.; Xie, L.; Kong, J.; Dresselhaus, M. S.; Zhang, J. Direct measurement of the Raman enhancement factor of rhodamine 6G on graphene under resonant excitation. *Nano Res.* **2014**, *7* (9), 1271−1279.
(18) Huang, S.; Ling, X.; Liang, L.; Song, Y.; Fang, W.; Zhang, J.; Kong, J.; Meunier, V.; Dresselhaus, M. S. Molecular Selectivity of Graphene-Enhanced Raman Scattering. *Nano Lett.* **2015**, *15* (5), 2892−2901.
(19) Rosa, A.; Baerends, E. J. metal macrocycle interaction in phthalocyanines-density-functional calculations of ground and excited-states. *Inorg. Chem.* **1994**, *33* (3), 584−595.
(20) Liao, M. S.; Scheiner, S. Electronic structure and bonding in metal phthalocyanines, Metal = Fe, Co, Ni, Cu, Zn, Mg. *J. Chem. Phys.* **2001**, *114* (22), 9780−9791.
(21) Xiao, K.; Liu, Y. Q.; Huang, X. B.; Xu, Y.; Yu, G.; Zhu, D. B. Field-effect transistors based on Langmuir-Blodgett films of phthalocyanine derivatives as semiconductor layers. *J. Phys. Chem. B* **2003**, *107* (35), 9226−9230.
(22) Farag, A. A. M. Optical absorption studies of copper phthalocyanine thin films. *Opt. Laser Technol.* **2007**, *39* (4), 728−732.
(23) Basova, T.; Kol'tsov, E.; Hassan, A.; Tsargorodskaya, A.; Ray, A.; Igumenov, I. Thin films of copper hexadecafluorophthalocyanine CuPcF16. *Phys. Status Solidi B* **2005**, *242* (4), 822−827.
(24) Liu, W.; Priddy, T. S.; Carlson, G. M. Physicochemical changes in phosphorylase kinase associated with its activation. *Protein Sci.* **2008**, *17* (12), 2111−2119.
(25) Kresse, G.; Furthmuller, J. Efficient iterative schemes for ab initio total-energy calculations using a plane-wave basis set. *Phys. Rev. B: Condens. Matter Mater. Phys.* **1996**, *54* (16), 11169−11186.
(26) Grimme, S.; Antony, J.; Ehrlich, S.; Krieg, H. A consistent and accurate ab initio parametrization of density functional dispersion correction (DFT-D) for the 94 elements H-Pu. *J. Chem. Phys.* **2010**, *132* (15), 154104.
(27) Hu, W.; Duan, S.; Zhang, Y.; Ren, H.; Jiang, J.; Luo, Y. Identifying the structure of 4-chlorophenyl isocyanide adsorbed on Au(111) and Pt(111) surfaces by first-principles simulations of Raman spectra. *Phys. Chem. Chem. Phys.* **2017**, *19* (48), 32389−32397.
(28) Hu, W.; Duan, S.; Luo, Y. Theoretical modeling of surface and tip-enhanced Raman spectroscopies. *Wiley Interdisciplinary Reviews-Computational Molecular Science* **2017**, *7* (2), No. e1293.
(29) Long, D. A. *The Raman Effect: A Unified Treatment of the Theory of Raman Scattering by Molecules*; Wiley Online Library, 2002; Vol. *1*.
(30) *Gaussian 03*, Revision C.02; Frisch, M. J.; Trucks, G. W.; Schlegel, H. B.; Scuseria, G. E.; Robb, M. A.; Cheeseman, J. R.; Montgomery, J. A., Jr.; Vreven, T.; Kudin, K. N.; Burant, J. C.; Millam, J. M.; Iyengar, S. S.; Tomasi, J.; Barone, V.; Mennucci, B.; Cossi, M.; Scalmani, G.; Rega, N.; Petersson, G. A.; Nakatsuji, H.; Hada, M.; Ehara, M.; Toyota, K.; Fukuda, R.; Hasegawa, J.; Ishida, M.; Nakajima, T.; Honda, Y.; Kitao, O.; Nakai, H.; Klene, M.; Li, X.; Knox, J. E.; Hratchian, H. P.; Cross, J. B.; Bakken, V.; Adamo, C.; Jaramillo, J.; Gomperts, R.; Stratmann, R. E.; Yazyev, O.; Austin, A. J.; Cammi, R.; Pomelli, C.; Ochterski, J. W.; Ayala, P. Y.; Morokuma, K.; Voth, G. A.; Salvador, P.; Dannenberg, J. J.; Zakrzewski, V. G.; Dapprich, S.; Daniels, A. D.; Strain, M. C.; Farkas, O.; Malick, D. K.; Rabuck, A. D.; Raghavachari, K.; Foresman, J. B.; Ortiz, J. V.; Cui, Q.; Baboul, A. G.; Clifford, S.; Cioslowski, J.; Stefanov, B. B.; Liu, G.; Liashenko, A.; Piskorz, P.; Komaromi, I.; Martin, R. L.; Fox, D. J.; Keith, T.; M. A., Al-Laham, Peng, C. Y.; Nanayakkara, A.; Challacombe, M.; Gill, P. M. W.; Johnson, B.; Chen, W.; Wong, M. W.; Gonzalez, C.; Pople, J. A. Gaussian, Inc.: Wallingford, CT, 2004.

DOI: 10.1021/acs.nanolett.8b04433
Nano Lett. 2019, 19, 1124−1130